Optimization of electrically tunable VCSEL with intracavity nematic liquid crystal

Carlos Belmonte,[1] Leszek Frasunkiewicz,[1,2] Tomasz Czyszanowski,[2] Hugo Thienpont,[1] Jeroen Beeckman,[3,4] Kristiaan Neyts,[3,4] and Krassimir Panajotov[1,5,*]

[1]*B-Phot., Vrije Universiteit Brussel Pleinlaan 2, 1050 Brussel Belgium*
[2]*Institute of Physics, Lodz University of Technology, Lodz 93-005, Poland*
[3]*Department of Electronics and Information Systems, Ghent University, Ghent 9000, Belgium*
[4]*Center of Nano and Biophotonics, Ghent University, Ghent 9000, Belgium*
[5]*Institute of Solid State Physics, 72 Tzarigradsko Chaussee blvd., 1784 Sofia, Bulgaria*
[*]*kpanajot@b-phot.org*

Abstract: We optimize the wavelength tuning range of a Vertical-Cavity Surface-Emitting Laser with an intracavity layer of nematic Liquid Crystal (LC-VCSEL) lasing around 1.3 μm. The tunability is obtained by applying voltage to the liquid crystal layer, which esentially is to vary the refractive index from the extraordinary to the ordinary. We achieve 71.6 nm continuous tuning (without mode hopping) with liquid crystal thickness of about 3.2 μm. We investigate the impact of ambient temperature on the LC-VCSEL tuning range and show that mode-hop tuning can be achieved in the temperature range from $-10\,^{\circ}$C to $50\,^{\circ}$C where the LC is in nematic phase.

OCIS codes: (140.3600) Lasers, tunable; (140.7260) Vertical cavity surface emitting lasers; (160.3710) Liquid crystals.

References and links

1. C. F. R. Mateus, M. C. Y. Huang, C. J. Chang-Hasnain, J. E. Foley, R. Beatty, P. Li, and B. T. Cunningham, "Ultra-sensitive immunoassay using VCSEL detection system," Electron. Lett. **40**, 649–651(2004).
2. M. Lewander, A. Fried, P. Weibring, D. Richter, S. Spuler, L. Rippe, "Fast and sensitive time-multiplexed gas sensing of multiple lines using a miniature telecom diode laser between 1529 nm and 1565 nm," Appl. Phys. B **104**, 715(2011).
3. M. Lackner, M. Schwarzott, F. Winter, B. Kogel, S. Jatta, H. Halbritter, and P. Meissner, "CO and CO2 spectroscopy using a 60 nm broadband tunable MEMS-VCSEL at 1.55 μm," Opt. Lett. **31**, 3170–3172(2006).
4. V. Jayaraman, J. Jiang, B. Potsaid, G. Cole, J. Fujimoto, and A. Cable, "Design and performance of broadly tunable, narrow line-width, high repetition rate 1310nm VCSELs for swept source optical coherence tomography," Proc. SPIE **8276**, 82760D (2012).
5. C. Gierl, K. Zogal, S. Jatta, H. A. Davani, F. Kuppers, P. Meissner, T. Grundl, C. Grasse, M.-C. Amann, A. Daly, B. Corbett, B. Kgel, A. Haglund, J. Gustavsson, P. Westbergh, A. Larsson, P. Debernardi, and M. Ortsiefer, "Tuneable VCSEL aiming for the application in interconnects and short haul systems," Proc. SPIE **7959**, 795908 (2011).
6. C.J. Chang-Hasnain, "Tunable VCSEL," IEEE J. Sel. Top. Quantum Electron. **6**, 978–987 (2000).
7. Y. Zhou, M. Huang, and C.J. Chang-Hasnain, "Tunable VCSEL with ultra-thin high contrast grating for high-speed tuning," Opt. Express **16**, 14221–14226 (2008).
8. R. Yi, Y. Weijian, C. Chase, M.C.Y. Huang, D.D.P. Worland, S. Khaleghi, M.R. Chitgarha, M. Ziyadi, A.E. Willner, and C.J. Chang-Hasnain, "Long-wavelength VCSEL using high-contrast grating," IEEE J. Sel. Top. Quantum Electron. **19** 1701311 (2013).

#234966 - $15.00 USD Received 19 Feb 2015; revised 17 Apr 2015; accepted 6 May 2015; published 5 Jun 2015

9. M.S Wu, E.C. Vail, G.S. Li, W. Yuen, and C.J. Chang-Hasnain, "Tunable micromachined vertical cavity surface emitting laser," Electron. Lett. **31**, 1671–1672 (1995).
10. D. Vakhshoori, P. Tayebati, C.-C. Lu, M. Azimi, P. Wang, J.-H. Zhou, and E. Canoglu, "2m WCW single-mode operation of a tunable 1550 nm vertical cavity surface emitting laser with 50 nm tuning range," Electron. Lett. **35**, 900–901 (1999).
11. A. Syrbu, V. Iakovlev, G. Suruceanu, C.-A. Berseth, A. Rudra, A. Mircea, A. Mereuta, and E. Kapon, "1 mW CW 38 nm tunable 1.5 μm VCSELS with tuning voltage below 4 V," Opt. Commun. **5**, 1–2 (2002).
12. A. Syrbu, V. Iakovlev, G. Suruceanu, A. Caliman, A. Rudra, A. Mircea, A. Mereuta, S. Tadeoni, C.-A. Berseth, M. Achtenhagen, J. Boucart, and E. Kapon, "1.55-μm optically pumped wafer-fused tunable VCSELs with 32-nm tuning range," IEEE Photon. Technol. Lett. **16**, 1991–1993 (2004).
13. V. Jayaraman, G. D. Cole, M. Robertson, A. Uddin, and A. Cable, "High-sweep-rate 1310 nm MEMS-VCSEL with 150 nm continuous tuning range," Electron. Lett. **48**, 867–869 (2012).
14. F. Riemenschneider, M. Maute, H. Halbritter, G. Boehm, M.-C. Amann, and P. Meissner, "Continuously tunable long-wavelength MEMS-VCSEL with over 40-nm tuning range," IEEE Photon. Technol. Lett. **16**, 2212–2214 (2004).
15. M. Maute, B. Kgel, G. Bohm, P. Meissner, and M.-C. Amann,"MEMS-tunable 1.55-μm VCSEL with extended tuning range incorporating a buried tunnel junction," IEEE Photon. Technol. Lett. **18**, 688–690 (2006).
16. S. Jatta, B. Kogel, M. Maute, K. Zogal, F. Riemenschneider, G. Bohm, M.-C. Amann, and P. Meisner, "Bulk-Micromachined VCSEL At 1.55 μm with 76-nm Single-Mode Continuous Tuning Range," IEEE Photon. Technol. Lett. **21**, 1822–1824 (2009).
17. C. Gierl, T. Gruendl, P. Debernardi, K. Zogal, C. Grasse, H. Davani, G. Bhm, S. Jatta, F. Kppers, P. Meiner, and M. Amann, "Surface micromachined tunable 1.55 μm-VCSEL with 102 nm continuous single-mode tuning," Opt. Express **19**, 17336–17343 (2011).
18. C. Gierl, K. Zogal, S. Paul, and F. Kppers, "Tunable MEMS-VCSEL with $>$ 140-nm tuning range using tuning range using SiO2/SiC-based MEMS-DBR," Proc. SPIE **9001**, 900107 (2014).
19. C. Levallois, B. Caillaud, J. de Bougrenet de la Tocnaye, L. Dupont, A. Lecorre, H. Folliot, O. Dehaese, and S. Loualiche, "Nano-polymer-dispersed liquid crystal as phase modulator for a tunable vertical-cavity surface-emitting laser at 1.55 μm," Appl. Opt. **45**, 8484–8490 (2006).
20. O. Castany, L. Dupont, A. Shuaib, J.P. Gauthier, C. Levallois, and C. Paranthoen, "Tunable semiconductor vertical-cavity surface-emitting laser with an intracavity liquid crystal layer," Appl. Phys. Lett. **98**, 161105 (2011).
21. O. Castany, C. Paranthoen, C. Levallois, A. Shuaib, J.P. Gauthier, N. Chevalier, O. Durand, L. Dupont, and A. Le Corre, "Demonstration of a 34 nm monolithic continuously tunable VCSEL at 1.55 μm combined with liquid crystal," Compound Semiconductor Week (CSW/IPRM), 23rd International Conference on Indium Phosphide and Related Materials (May 2011) pp. 1–4.
22. Y. Xie, J. Beeckman, W. Woestenborghs, K. Panajotov, and K. Neyts, "VCSEL with photo-aligned liquid crystal overlay," IEEE Photon. Technol. Lett. **24**, 1509–1512 (2012).
23. Y. Xie, J. Beeckman, K. Panajotov, and K. Neyts, "Vertical-cavity surface-emitting laser with a liquid crystal external cavity," Opt. Lett. **39**, 6494–6497 (2014).
24. K. Panajotov and H. Thienpont, "Vertical-cavity surface-emitting laser with liquid crystal overlay," Opt. Express **19**, 16749–16759 (2011).
25. K. Panajotov, Y. Xie, M. Dems, C. Belmonte, H. Thienpont, J. Beeckman, K. Neyts, "Vertical-cavity surface-emitting laser emitting circularly polarized light," Laser Phys. Lett. **10**, 105003 (2013).
26. Y. Xie, J. Beeckman, K. Panajotov, K. Neyts, "Vertical-cavity surface-emitting laser with a chiral nematic liquid crystal overlay, IEEE Photon. J. **6**, 1500010 (2014).
27. N. Volet, T. Czyszanowski, J. Walczak, L. Mutter, B. Dwir, Z. Mickovi, P. Gallo, V. Iakovlev, A. Sirbu, A. Caliman, A. Mereuta, and E. Kapon, "Improved single-mode emission characteristics of long-wavelength wafer-fused vertical-cavity surface-emitting lasers by intra-cavity patterning," Proc. SPIE **8639**, 86390S (2013).
28. X.H. Li, V.M. Kozenkov, F.S.Y. Yeung, P.Z. Xu, V.G. Chigrinov, and H.S. Kwok, "Liquid-crystal photoalignment by super thin azo dye layer," Jpn. J. Appl. Phys. **45**, 203–205 (2006).
29. M. Born and E. Wolf, *Principles of Optics* (Wiley, 1970).
30. J. Li, S.-T. Wu, S. Brugioni, R. Meucci, and S. Faetti, "Infrared refractive indices of liquid crystals," J. Appl. Phys. **97**, 073501 (2005).
31. J. Li, C. Wen, S. Gauza, R. Lu, and S. Wu, "Refractive indices of liquid crystals for display applications," J. Display Technol. **1**, 51 (2005).
32. T. Czyszanowski, M. Dems, R. Sarzaa, K. Panajotov, K. D. Choquette, "Photonic crystal VCSELs: detailed comparison of experimental and theoretical spectral characteristics," IEEE J. Sel. Top. Quantum Electron. **19**, 1701908 (2013).
33. R. Sarzala, T. Czyszanowski, M. Wasiak, M. Dems, L. Piskorski, W. Nakwaski, K. Panajotov, "Numerical self-consistent analysis of VCSELs advances in optical technologies," Advances in Optical Technologies **2012**, 689519 (2012).
34. T. Czyszanowski, M. Dems, K. Panajotov, "Single mode condition and modes discrimination in photonic-crystal

#234966 - $15.00 USD Received 19 Feb 2015; revised 17 Apr 2015; accepted 6 May 2015; published 5 Jun 2015

1.3 μm AlInGaAs/InP VCSEL," Opt. Express **15**, 5604 (2007)
35. T. Czyszanowski, N. Volet, J. Walczak, M. Dems, R.P. Sarzala, V. Iakovlev, A. Sirbu, A. Mereuta, A. Caliman, E. Kapon, "Numerical analysis of mode discrimination by intracavity patterning in long-wavelength wafer-fused vertical-cavity surface-emitting lasers," IEEE J. Quantum Electron. **50**, 732–740 (2014).

1. Introduction

Tunable semiconductor lasers operating in the wavelength region around 1310 nm and 1550 nm are of great interest for various applications, such as biological and gas sensing [1, 2], spectroscopy [3], tomography [4] or telecommunications [5–8]. Many groups have demonstrated wavelength tuning of electrical or optically pumped VCSEL combined with Micro-Electro-Mechanical-System (MEMS) technology, using a moving membrane like a mirror to change the optical cavity length and hence provide wavelength tuning. MEMS movable reflector are typically cantilever or membrane structures using high contrast gratings or DBRs and are actuated by electrostatic, electrothermal or piezo-electric forces.

MEMS-VCSEL, in which the top DBR comprises a micromachined cantilever (c-VCSEL), was first demonstrated in 1995 in [9]. Wavelength tuning range (TR) of 15 nm was achieved for a voltage of 5.7 V. In 1999, a tunable 1.55 μm VCSEL with a 50 nm TR was developed [10]. The device top membrane with a curved mirror is pulled down by electrostatic force, when applying voltage from 0 to 39 V between the top membrane and the bottom mirror. In 2002, a wafer-fused optically pumped tunable VCSEL with output power up to 1 mW at 1.55-μm and 38 nm TR for a voltage change of 4 V was reported [11]. In 2004, the same group achieved an output power of 2 mW reducing the TR to 32 nm for a voltage below 4 V [12]. TR is further increased to 150 nm in optically pumped MEMS-VCSEL around 1.3 μm in 2012 [13].

For the first time, an electrically pumped tunable MEMS-VCSEL with a TR of 40 nm and a maximum output power of 100 μW was developed in 2004 [14]. The VCSEL is based on a two-chip concept, where the movable mirror membrane is fabricated on a separate chip, avoiding compromise between MEMS and VCSEL designs. Using a similar device, the same group improved the output power up to 1.7 mW by reducing the top mirror reflectivity, but reduced the TR till 28 nm [15]. The TR is significantly increased to 60 nm in 2006 [15] and to 76 nm in 2009 [16] using an antireflection coatings. The upper MEMS mirror is a SiO_2-SiN concave DBR which can be actuated electrothermally. The maximum output power measured is 1.31 mW. A high performance electrically pumped single-mode MEMS tunable VCSEL with a TR of 102 nm with a maximum output power of 3.2 mW was developed in 2011 [17]. The technology used is based on low temperature plasma enhanced chemical vapor deposition without wafer-bonding or wafer-gluing and is not restricted to 1.55 μm only. The SiO_x-SiN_y based movable top DBR is a membrane, which is suspended on four flexible beams. When the current flows through the metallization of the top mirror membrane, the beams of the membrane are expanded, increasing the air-gap cavity length. The largest TR of 140 nm for electrically pumped MEMS-VCSEL was reported in 2014 [18]. The tunable VCSEL is based on the same structure as in [17] however, with high refractive index contrast SiO_2/SiC layers movable DBR that broadens the spectral width of the reflectivity and increases the TR.

Despite the excellent and large TR, MEMS tunable VCSELs suffer from a rather complex technological process, and the separate MEMS are sensitive to mechanical vibrations. Another way to obtain wavelength tuning in VCSELs is to change its refractive index, using LC as an electro-optic material located in the cavity, forming a device without any movable part. LC-VCSELs have many advantages, such as simpler technological process, insensitivity to mechanical disturbances, small tuning response time and high reliability. A nonmechanical tunable VCSEL with a nematic LC using optical pumping was first demonstrated in 2006 [19]. The TR was 10 nm with a tuning response time of 30 μs applying a voltage of 150 V. The

#234966 - $15.00 USD Received 19 Feb 2015; revised 17 Apr 2015; accepted 6 May 2015; published 5 Jun 2015

structure is composed of 7 InGaAs/InGaAsP quantum wells, InP/AnGaAsP bottom DBR and SiO_2/TiO_2 top DBR, grown on InP substrate. The same group presented in 2011 [20] a tunable VCSEL with a nematic LC in the 1.5 μm wavelength regime under optical pumping, with a TR of 33 nm with less than 3 V applied voltage. The structure is composed of 8 InGaAs/InGaAsP quantum wells, amorphous-Si/amorphous-SiN bottom DBR and SiO_2/TiO_2 top DBR. In 2011, an optically pumped 1.55 μm emitting tunable VCSEL using intracavity nematic LC (BL036), achieved a TR of 34 nm for a voltage change of 2.4 V [21].

Recently, we have developed technology for integration of a VCSEL chip into an LC cell [22]. Based on this technology we have shown that coupled-cavity LC-VCSEL device can be efficiently used for polarization control and polarization switching by changing the voltage applied to the LC [23] thus confirming the theoretical results of [24]. Furthermore, with a chiral LC such LC-VCSEL generates circularly rather than linearly polarizaed light with lower threshold current and enhanced degree of polarizatoion [25, 26].

Because of these impressive achievements, question arises if the TR of intracavity LC-VCSEL can be further increased, especially for structures that allow for electrical pumping. We answer this question here, by carrying out an optimization of an LC-VCSEL lasing around 1.31 μm and achieve a TR of 71.6 nm. Furthermore, we investigate the impact of temperature on the TR and show that mode-hop free TR can be maintained from $-10\,^{\circ}$C to $50\,^{\circ}$C for LC thickness of 2.7 μm on the expense of decreasing the TR from 77.2 nm at $-10\,^{\circ}$C to 38.2 nm at $50\,^{\circ}$C.

2. Device structure

In Fig. 1 a schematic cross section of the tunable LC-VCSEL is shown, with the LC placed in-between a Half VCSEL (bottom DBR and Active Region) and a top DBR.

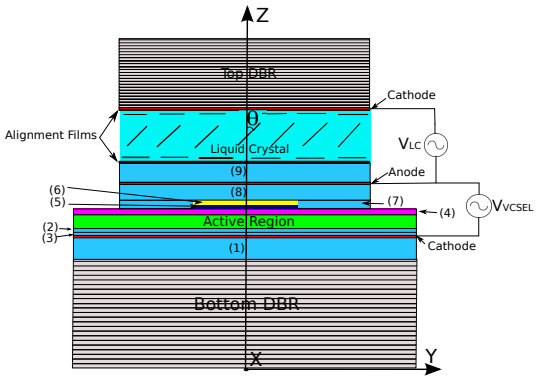

Fig. 1. Schematic of the cross section of a tunable LC-VCSEL with intracavity nematic LC. Detailed description of the structure with labels denoted is given in Table 1.

Our structure is based on [27], where a wafer-fusion VCSEL has been optimized for low threshold current and wide stop-band of more than 100 nm. The bottom DBR consists of 35 pairs of nid $GaAs/Al_{0.9}Ga_{0.1}As$. The bottom DBR is wafer-fused to a $5/2\lambda$ cavity grown on an InP substrate. The active region consists of six compressively strained AlGaInAs QWs with seven tensile strained barriers of AlGaInAs. The p-doped AlInAs layer acts as a current blocking layer and is followed by a buried highly doped P+ N+ tunnel junction. On top of the N-InP spacer we place the LC layer sandwiched between two alignment layers of azo dye SD1 [28]. The top DBR consists of N_{top} = 25 pairs of nid-$GaAs/Al_{0.9}Ga_{0.1}As$ and 1 pair of n-doped (N = $5 \cdot 10^{18}$ cm^{-3}) $GaAs/Al_{0.9}Ga_{0.1}As$. We also study the cases with N_{top} = 20 and N_{top} = 16.

#234966 - $15.00 USD Received 19 Feb 2015; revised 17 Apr 2015; accepted 6 May 2015; published 5 Jun 2015

Finally, two intracavity highly doped contact layers achieve a proper electrical injection. The doped layer in the top DBR acts as a third intracavity contact, which is used to apply a voltage to the LC. The detailed description of the LC-VCSEL structure is presented in Table 1.

Table 1. Detailed structure of the LC-VCSEL.

	Material	**Doping [cm^{-3}]**	L **[nm]**	**n**	**Description**
	GaAs	nid	96	3.41 - i10^{-4}	Top DBR
x25	$Al_{0.9}Ga_{0.1}As$	nid	109.9	2.98 - i10^{-4}	Top DBR
	GaAs	nid	96	3.41 - i10^{-4}	Top DBR
x1	$Al_{0.9}Ga_{0.1}As$	$N = 5 \cdot 10^{18}$	109.9	2.99 - i0.00016	Cathode Contact
	GaAs	$N = 5 \cdot 10^{18}$	96	3.41 - i0.00024	Cathode Contact
	SD1	nid	2	3.2	Alignment Layer
	Liquid Crystal	nid	L (LC)	n_e, n_o	Liquid crystal
	SD1	nid	2	3.2	Alignment Layer
	InP	$N = 10^{18}$	197.5	3.2 - i10^{-5}	(9)
	GaInPAs	$N = 5 \cdot 10^{18}$	15	3.4 - i0.16	Anode Contact
	InP	$N = 10^{18}$	182	3.2 - i10^{-5}	(8)
	InP	$N = 10^{18}$	30	3.2 - i10^{-5}	(7)
	AlGaInAs	$N = 5 \cdot 10^{19}$	15	3.4 - i0.006	(6)
	AlGaInAs	$P = 5 \cdot 10^{19}$	15	3.4 - i0.006	(5)
	AlInAs	$P = 2 \cdot 10^{18}$	40	3.25 - i10^{-5}	(4)
x6	AlGaInAs	nid	6.7	3.3	Barrier
	AlGaInAs	nid	6	3.6	Well
	AlGaInAs	nid	6.7	3.3	Barrier
	InP	nid	20	3.2 - i10^{-10}	(3)
	InP	$N = 1.5 \cdot 10^{18}$	27.7	3.2 - 2.4$\cdot i10^{-5}$	(2)
	GaInPAs	$N = 5 \cdot 10^{18}$	15	3.4 - i0.16	Cathode Contact
	InP	$N = 10^{18}$	402.5	3.2 - i10^{-5}	(1)
x35	GaAs	nid	96	3.41 - i10^{-4}	Bottom DBR
	$Al_{0.9}Ga_{0.1}As$	nid	109.9	2.98 - i10^{-4}	Bottom DBR
	GaAs	nid	inf	3.41 - i10^{-4}	Substrate

The current is uniformly distributed thanks to N-doped InP layers (1) and (2) before injection into the cavity starting with the nid InP layer (3). The layers (4) and (7) (P-AlInAs and N-InP, respectively) are spacers to adjust the tunnel junction. A uniform current injection is necessary for avoiding any filamentation of the lasing mode, which is why the current injected into the tunnel junction is spread by the N-doped spreading layers (8) and (9). Layers (1) and (9) are much thicker than the rest of the layers and are used for fine tuning the cavity thickness for the emission wavelength. In our device the tunnel junction consists of two AlGaInAs layers of 15 nm; the first one is N-type doped (N = $5 \cdot 10^{19}$ cm^{-3}) and the second is P-type doped (P = $5 \cdot 10^{19}$ cm^{-3}). We implement a nematic E7 LC placed between the layer (9) and the top DBR. The layer of the top DBR in contact with the LC is highly-doped and it is the cathode contact to apply the voltage to the LC. Alignment layers are required on both sides of the LC to control the orientation of its molecules. When a voltage is applied to the LC, its molecules tilt from a planar to a nearly homeotropic orientation which means that the refractive index goes from the extraordinary to the ordinary, and the laser emission wavelength of the LC-VCSEL decreases.

#234966 - $15.00 USD Received 19 Feb 2015; revised 17 Apr 2015; accepted 6 May 2015; published 5 Jun 2015

3. Theoretical results

Our procedure of optimizing the LC-VCSEL for large TR is based on the transfer matrix method [24, 29] to find the resonant wavelengths and the corresponding threshold gains. Three different variables of our structure are varied: the LC thickness, the number of pairs in the top DBR and the transition from the extraordinary refractive index (n_e) to the ordinary refractive index (n_o) of the LC when voltage is applied. This transition will determine the tuning spectra of our LC-VCSEL. The refractive indices for light traveling along Z axis and linearly polarized along the X and Y axes are determined by [24]

$$\begin{aligned} n_x &= n_o, \\ n_y &= \frac{n_o n_e}{\sqrt{n_o^2 sin^2(\theta) + n_e^2 cos^2(\theta)}}, \end{aligned} \tag{1}$$

where θ is the angle at which the molecules are aligned with respect to the z axis. We carry out the optimization procedure by performing a sweep of the LC thickness, with fixed number of DBR and refractive index of the LC, either the ordinary or the extraordinary (n_o or n_e). Figure 2 shows the evolution of the lowest threshold gain mode and the corresponding resonance wavelength, with the thickness of the LC. The number of pairs of the top DBR is fixed to 25.

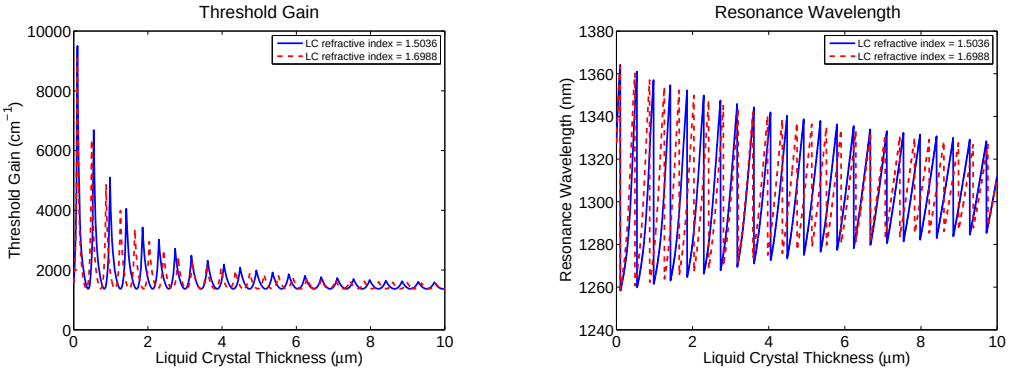

(a) (b)

Fig. 2. Threshold gain (a) and resonance wavelength (b) of the lasing mode as a function of the LC thickness. The solid blue curve corresponds to the ordinary refractive index (n_o) and the dashed red line to the extraordinary refractive index (n_e). The number of pairs of the top DBR is N_{top} = 25.

The period of the solid blue curve for the ordinary refractive index (n_o=1.5036) is 440 nm and for the dashed red line for extraordinary refractive index (n_e=1.6899) is 387 nm, which correspond to half of the optical wavelength of λ_0 = 1.31μm ($n_o L_o \approx n_e L_e \approx \lambda_0/2$). Due to the fact that the two periods are different, there is a situation when the peaks for the n_o and n_e refractive indices coincide (e.g. at L $\approx$ 3.3 μm and L $\approx$ 6.6 μm). This modulation is better seen in Fig. 3 where the differences between the two curves from Fig. 2 are shown. The periodicity of the envelope of the modulation in Fig. 3 corresponds to L = 3.51 μm, which is given approximately by $L \approx \lambda/(2(n_e\text{-}n_o))$. From Fig. 3 is clearly seen that the maximum mode-hop free TR of about 71.6 nm occurs when the LC thickness is around 3.2 μm.

#234966 - $15.00 USD Received 19 Feb 2015; revised 17 Apr 2015; accepted 6 May 2015; published 5 Jun 2015

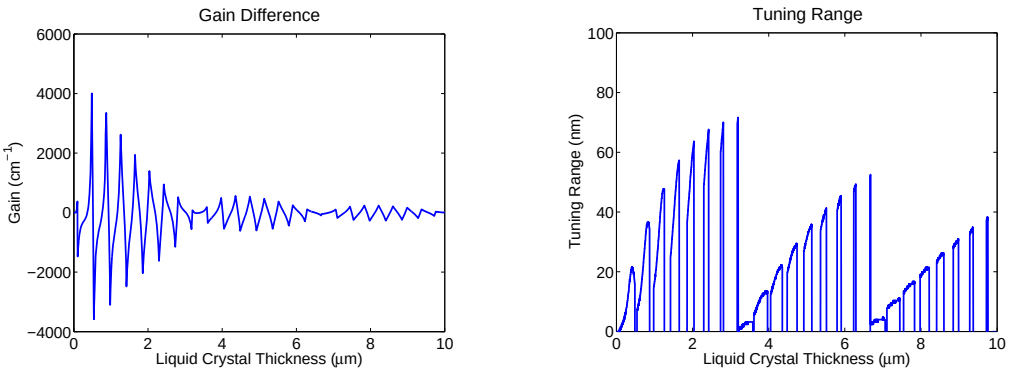

(a) (b)

Fig. 3. Gain difference (a) and TR (b) as a function of the LC thickness. These figures are obtained by subtracting the two curves for n_e and n_o in Fig. 2.

A comparison of the three threshold gains corresponding to the maximum TR as a function of the LC refractive index for different numbers of top DBR (25, 20 and 16) can be seen in Fig. 4(a). The TR as a function of the LC refractive index for the three different cases is shown in Fig. 4(b). As can be seen, the lowest threshold gain with the largest TR is achieved with N_{top} = 25 pairs. Quite importantly, the TR is not strongly impacted by the reflectivity of the top mirror, remaining approximately around 72 nm.

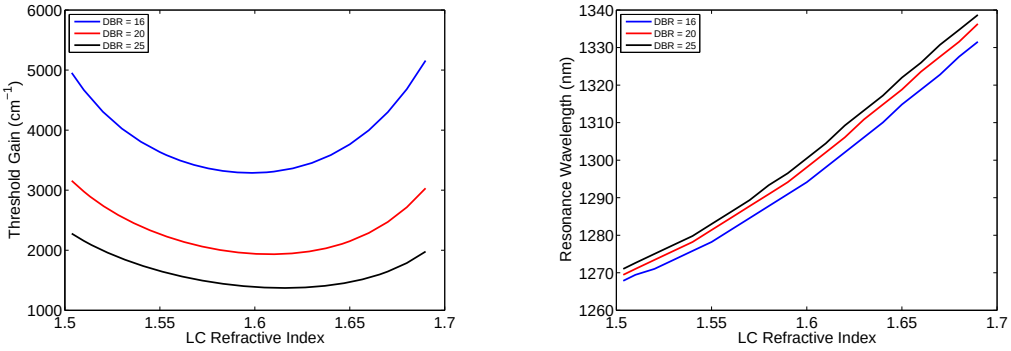

(a) (b)

Fig. 4. Threshold gain (a) and resonance wavelength (b) as a function of LC refractive index for three different number of DBR pairs. The black curve corresponds to N_{top} = 25 with a LC thickness fixed to 3.2 μm and the maximum TR is 71.6 nm. The red curve corresponds to N_{top} = 20 with a TR of 70 nm and LC thickness of 3.18 μm. Finally the blue curve corresponds to N_{top} = 16 with a TR of 67.6 nm and LC thickness of 3.16 μm.

4. Temperature effects on the LC-VCSEL wavelength tuning range

In this section we study the temperature effects on the LC refractive indices and therefore, on the TR. In a homogeneous cell, the LC exhibits two refractive indices, n_e and n_o, depending on the incident light polarization, respectively, parallel or perpendicular to the LC director. Birefringence (Δn) is the difference between these two refractive indices; i.e. Δn = n_e - n_o.

#234966 - $15.00 USD Received 19 Feb 2015; revised 17 Apr 2015; accepted 6 May 2015; published 5 Jun 2015

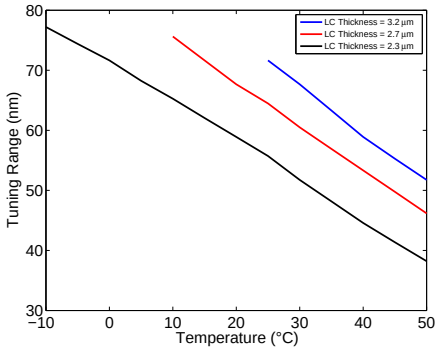

Fig. 5. Wavelength TR comparison for different thicknesses of the intracavity LC for a range of temperatures from $-10\,^{\circ}$C to $50\,^{\circ}$C.

We use commercial E7 LC from Merck, with high birefringence of Δn = 0.1863 at $25\,^{\circ}$C. The temperature range of nematic LC phase is between the melting temperature of $-10\,^{\circ}$C and the clearing temperature of $60\,^{\circ}$C [30]. To calculate the refractive indices of the LC as a function of wavelength, we use the Cauchy Eqs. (2). For LC compounds with high birefringence, like the E7, the three-band model equations. are the ones that fit better the experimental results [31], namely

$$n_{e,o} \cong A_{e,o} + \frac{B_{e,o}}{\lambda^2} + \frac{C_{e,o}}{\lambda^4}, \tag{2}$$

where $A_{e,o}$, $B_{e,o}$, and $C_{e,o}$ are the Cauchy coefficients which are constants, independent on wavelength, but dependent on the temperature. The value of the Cauchy coefficients at $25\,^{\circ}$C are taken from [30]; A_e = 1.6933, B_e = 0.0078, C_e = 0.0028 and A_o = 1.4994, B_o = 0.0070, C_o = 0.0004. From Eq. (2), we can obtain the refractive indices of the E7 at $25\,^{\circ}$C as n_o = 1.5036 and n_e = 1.6899. Although the range of temperatures in which the LC of E7 is in the nematic phase is from $-10\,^{\circ}$C to $60\,^{\circ}$C, near the clearing temperature the values of the refractive indices change drastically, in nonlinear fashion. Therefore we set the range of temperatures under study from $-10\,^{\circ}$C to $50\,^{\circ}$C, where the refractive indices have a linear dependence on temperature, characterized by the thermooptic coefficients

$$\beta_{e,o} = dn_{e,o}/dT \tag{3}$$

From [30] we know the values of the Cauchy coefficients at $45\,^{\circ}$C, i.e. A_e = 1.6565, B_e = 0.0083, C_e = 0.0024 and A_o = 1.5018, B_o = 0.0068, C_o = 0.0006. Using Eq. (2), we obtain the refractive indices for E7 at $45\,^{\circ}$C, n_o = 1.5059 and n_e = 1.6621. Knowing the refractive indices for $25\,^{\circ}$C and $45\,^{\circ}$C, the thermooptic coefficients can be easily obtained using Eq. (3) (β_e = -1.835·10^{-3} and β_o = 1.15·10^{-4}). In such way, the refractive indices for different temperatures can be calculated from:

$$n_{e,o}(T_0 + \Delta T, \lambda) = n_{e,o}(T_0, \lambda) + \beta_{e,o}\Delta T \tag{4}$$

From Fig. 3 it can be seen that the maximum TR occurs when the thickness of the LC is around 3.2 μm. To study the temperature effect on the wavelength tuning, we take this thickness and check the TR from $-10\,^{\circ}$C to $50\,^{\circ}$C. Figure 5 shows the TR for three different LC

#234966 - $15.00 USD Received 19 Feb 2015; revised 17 Apr 2015; accepted 6 May 2015; published 5 Jun 2015

thicknesses of L_{LC} = 3.2 μm, 2.7 μm and 2.3 μm, where we obtain a mode-hop free TR in temperature ranges of ΔT = 25 °C, 40 °C and 60 °C, respectively. As can be seen, mode-hop free TR can be maintained from -10 °C to 50 °C for LC thickness of 2.7 μm on the expense of decreasing the TR from 77.2 nm at -10 °C to 38.2 nm at 50 °C.

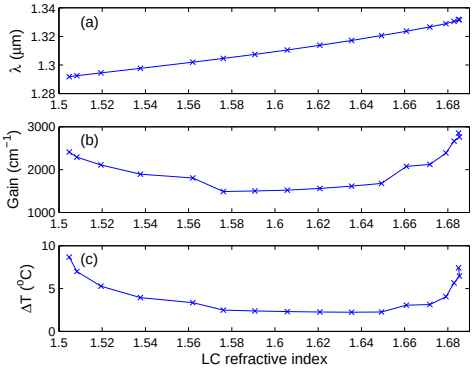

Fig. 6. Resonant wavelength (a), thresholds gain (b) and maximal temperature rise ΔT in the LC above the ambient temperature (c) as a function of LC refractive index obtained by self-consistent electro-thermal-optical LC-VCSEL model. The LC thickness is $L = 2.315\mu$m and the tunnel junction aperture radius is $R_{TJ} = 3.5\mu$m.

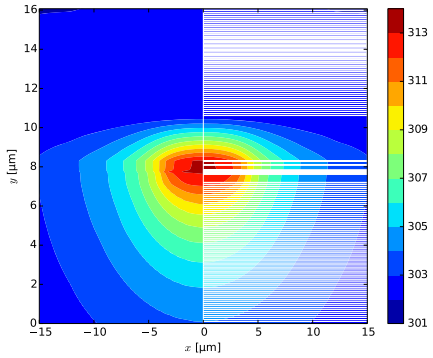

Fig. 7. Temperature distribution in a vertical cross-section of the LC-VCSEL for the extraordinary LC refractive index at the threshold current of I_{th} = 6.43 mA. On the left side the LC-VCSEL layered structure is shown by white lines: the LC occupies the large uniform part between 8 μm and 10 μm.

In the calculation method employed so far the internal heating of the VCSEL by the injection current has not been taken into account. Question therefore arises if this heating can prevent the wavelength tuning when electro-optically changing the LC refractive index. In order to answer this question, we have carried out 3D calculation of the LC-VCSEL system that accounts self-consistently for the injection current distribution, generated temperature distribution, its impact on the gain and the resonant optical mode at the lasing threshold [32–34]. The model was already used in simulations of similar structures and revealed very good agreements with experiment [35]. Example of such calculations for LC thickness of 2.315 μm is presented in

#234966 - $15.00 USD Received 19 Feb 2015; revised 17 Apr 2015; accepted 6 May 2015; published 5 Jun 2015

Fig. 6, where the top panel presents the resonant wavelength, the middle panel the thresholds gain and the bottom panel the temperature rise in the LC above the ambient temperature as a function of LC refractive index. As can be seen from Fig. 6(a), the wavelength tuning properties of the LC-VCSEL are reproduced well by these self-consistent calculations revealing threshold gain change with LC refractive index (Fig. 6(b)), similar to the one in Fig. 4(a) obtained by the simple 1D optical solver. Quite importantly, the self-consistent LC-VCSEL model reveals that the temperature rise in the LC layer is only about 10°C for a current of 6.43 mA (Fig. 6(c)) and can not therefore impact severely the wavelength tuning properties of LC-VCSEL system. Finally, Fig. 7 shows an example of temperature distribution in a vertical cross-section of the LC-VCSEL. In the intracavity contacted VCSEL considered here, heat is generated close to the active region and is mostly vertically transferred to the bottom DBR and the substrate and spread laterally in the semiconductor material.

5. Conclusion

An optimization has been carried out to achieve the maximum wavelength tuning range (TR) of a VCSEL lasing around 1.3 μm with an intracavity nematic LC (E7). A TR of 71.6 nm at room temperature (25 °C) is obtained for a LC thickness of 3.2 μm: when the refractive index of the LC goes from the extraordinary to the ordinary the laser emission wavelength decreases from 1342.7 nm to 1271 nm. The threshold gain remains lower than 2500 cm^{-1} (3200 cm^{-1}) in the whole TR for a top DBR with N_{top} = 25 (20) pairs. Decreasing the top DBR reflectivity increases the threshold gain, however it does not impact the tuning range. We have also checked the impact of the ambient temperature on the tuning range. For the E7 LC studied here, the temperature range of the nematic phase is from $-10\,^{\circ}$C to 60 °C. We have shown that a mode-hop free TR can be maintained from $-10\,^{\circ}$C to 50 °C for LC thickness of 2.7 μm on the expense of decreasing the TR from 77.2 nm at $-10\,^{\circ}$C to 38.2 nm at 50 °C. Finally, we ascertain our findings by a 3D calculation of the LC-VCSEL system that accounts self-consistently for the injection current distribution, generated temperature distribution, its impact on the gain and the resonant optical mode at the lasing threshold.

Acknowledgments

The authors acknowledge the financial support of FWO-Vlaanderen project G.0656.09N and the Interuniversity Attraction Poles program of the Belgian Science Policy Office, under grant IAP P7-35 photonics@be. K.P. acknowledges project DFNI-T02/18 of Bulgaria National Science Fund. H. T. and K. P. are grateful to the Methusalem foundation for financial support. This work was also supported in part by the Polish National Science Centre, Project DEC-2012/06/M/ST7/00442.

#234966 - $15.00 USD Received 19 Feb 2015; revised 17 Apr 2015; accepted 6 May 2015; published 5 Jun 2015